JURNAL ECOTIPE
Electronic, Control, Telecommunication, Information, and Power Engineering

Volume 11, Issue 2, October 2024, pp. 224-234
ISSN 2355-5068 ; e-ISSN 2622-4852
DOI: 10.33019/jurnalecotipe.v11i2.4523

Enhanced Depth Control and Stability in Submersible Pylon Inspection Robots Using IMU-Based Extended Kalman Filter and PID Control

Hendi Purnata[1], Riyani Prima Dewi[2], Saepul Rahmat[3], Erna Alimudin[4], Novita Asma Ilahi[5]
[1]Mechatronics Engineering, Cilacap State of Polytechnic, Jl. Dr. Soetomo No. 1, Cilacap 53212, Indonesia
[2,3,5]Electrical Engineering, Cilacap State of Polytechnic, Jl. Dr. Soetomo No. 1, Cilacap 53212, Indonesia
[4]Electronics Engineering, Cilacap State of Polytechnic, Jl. Dr. Soetomo No. 1, Cilacap 53212, Indonesia

ARTICLE INFO

Article history:

Received: 19/08/2024
Revised : 26/08/2024
Accepted: 17/10/2024

Keywords:

Depth Control; Extended Kalman Filter; Inertial Measurement Unit; Proportional Integral Derivative; Stability; Underwater Robot

ABSTRACT

This research develops a Submersible Pylon Inspection Robot (SPIR) equipped with an Inertial Measurement Unit (IMU) and Extended Kalman Filter (EKF) to improve stability and depth control in dynamic underwater environments. The implemented control system uses a customized PID algorithm to optimize the depth response. Results show that SPIR is able to maintain depth well at shallow depths, but struggles to maintain stability at deeper depths, especially when encountering strong currents. Large fluctuations in the z-axis and position deviation at deeper depths indicate the need for refinement of the PID control algorithm, including the possible use of advanced control or prediction-based control to cope with dynamic environmental conditions. In addition, the integration of IMU and EKF showed good performance in reducing noise in the sensor data, but challenges arose in the early phase of measurement, where large fluctuations in the quaternion angle indicated the initial instability of the sensor. Therefore, it is recommended to make further adjustments to the EKF parameters to accelerate convergence and reduce sensor noise. This research shows that with further refinements to the sensor control and integration, SPIR can be an effective tool for underwater inspection operations at more extreme conditions.

Corresponding Author:

Hendi Purnata
Electronics Engineering, Cilacap State of Polytechnic, Jl. Dr. Soetomo No. 1, Cilacap 53212, Indonesia
Email: hendipurnata@pnc.ac.id

1. INTRODUCTION

In recent decades, advances in marine technology have triggered a growing interest in the exploration and exploitation of marine resources, especially in maritime countries such as Indonesia with vast marine areas [1]. However, the complexity of marine robotics, including high cost, large size, and significant weight, is a major obstacle in the development of this technology. The sinking of submarine 402 in April 2021, which was caused by natural factors such as underwater currents, shows the urgency of developing underwater technology to strengthen Indonesia's marine security [2]. Rapid advances in marine science and technology over the past two decades have fueled a growing interest in the exploration and exploitation of the oceans for scientific and commercial purposes. In this context, marine robotics has emerged as a key technology to carry out increasingly complex and challenging missions at sea. Although there have been significant advances in methodologies and applications, major

Volume 11, Issue 2, October 2024, pp. 224-234
ISSN 2355-5068 ; e-ISSN 2622-4852
DOI: 10.33019/jurnalecotipe.v11i2.4523

challenges remain, requiring further research and development to meet the requirements of the next generation of marine robots and their support systems [3-5].

Despite the progress that has been made, major challenges such as depth control and stability still hinder the development of underwater vehicles. Some research, such as the development of the Submersible Pylon Inspection Robot (SPIR), has focused on improving automation to reduce human involvement in hazardous conditions. SPIR uses SONAR-based navigation and 3D reconstruction, but still faces difficulties in controlling depth, especially in environments with strong currents [6]. In marine environments, effective depth control on underwater vehicles faces significant challenges due to the reliance on navigation and communication systems that often suffer from limitations in range and latency. The integration of unmanned systems, such as UAVs, can offer potential solutions to improve connectivity and resource management with great flexibility, but also introduces new complexities in data management and dynamic control. Despite the progress made in the automation of underwater vehicle docking and navigation systems, there is still an urgent need to overcome these constraints, including the adaptation to non-specially designed docking systems as well as the application of new technologies in extreme environments [7-8]

Similar challenges are also encountered in the control of Remotely Operated Vehicles (ROVs), where reliance on limited sensors in a dynamic environment often leads to depth and position estimation errors [9-11].This paper highlights the importance of advanced methods and techniques for depth control in underwater Remotely Operated Vehicles (ROVs). Given the wide maritime and industrial applications, including repair, the maintenance of precise depth control is crucial. The methods proposed in this study, such as a robust H∞ depth tracking controller with an innovative event-triggering method, the use of a tether to measure hydrodynamic forces without interference, as well as a fuzzy PID strategy with dynamic compensation, all aim to improve ROV accuracy and stability under complex environmental conditions. Experimental results show that these approaches are effective in reducing depth errors, minimizing the influence of disturbances, and optimizing ROV performance, which are indispensable for meeting the requirements of practical applications in various sectors.

The use of Inertial Measurement Unit (IMU) and Extended Kalman Filter (EKF) in depth control has been an active research area, but current technologies still face limitations in terms of accuracy and stability. In an effort to improve accuracy, several studies have proposed multi-sensor fusion systems that combine data from IMUs, pressure sensors, optical flow, and ArUco markers to obtain more precise positions and reduce location drift over time. In addition, techniques such as the combination of short baseline (SBL) and inverted ultrashort baseline (iUSBL) measurements using EKF have been applied in underwater mining scenarios to overcome localization challenges in confined environments. Orientation estimation with EKF is also used in Autonomous Underwater Vehicles (AUVs) to update position estimation under magnetic disturbance conditions, by combining data from GPS, Doppler Velocity Log (DVL), and Fiber Optic Gyroscope (FOG). Although these approaches show promising results, further development is needed to achieve more accurate and stable depth control in various environmental conditions [12-13]. However, these methods still have limitations in terms of accuracy and adaptability under rapidly changing environmental conditions.

The use of MEMS-based nine-axis Inertial Measurement Units (IMUs) has been widely applied in various fields, such as underwater vehicles, unmanned aerial vehicles, and bionic robots. However, due to the noise in gyroscope sensors and errors in the solution process, the rotation angle estimated with only angular velocity data usually contains large accumulated errors and must be corrected by acceleration and geomagnetic measurements. A serious problem arises if there are strong magnetic field anomalies in the environment, which can degrade the performance of geomagnetic field correction and add errors. To improve the heading and attitude estimation accuracy of the nine-axis MEMS IMU in magnetic field anomalies, this study proposes the use of a partially adaptive Extended Kalman Filter (EKF) (PADEKF) with dual quaternions. To reduce the connected influence of magnetic measurement noise on attitude estimation in one quaternion, the heading angle and attitude are represented with two independent quaternions in the state vector. A self-adaptability design is adopted in EKF to improve robustness to spatially varying magnetic anomaly data. In the case of strong and fast-varying magnetic anomaly fields that cannot be well modeled by PADEKF, a combination algorithm of LSTM neural

Volume 11, Issue 2, October 2024, pp. 224-234
ISSN 2355-5068; e-ISSN 2622-4852
DOI: 10.33019/jurnalecotipe.v11i2.4523

network and Runge-Kutta method is given to obtain a good heading estimation. Field experiments in various scenarios are conducted and verify the effectiveness of the proposed approach [14].

PID control methods are frequently used in autonomous underwater vehicle (AUV) depth control, but they are often unable to cope with significant depth fluctuations or adapt to dynamic changes in the underwater environment. For example, in the proposed study, PID control is used to regulate the propeller rotation of a fast-moving AUV in a horizontal orientation and then rotate downward to float at the desired water depth. Although PID control can execute depth control maneuvers, this approach is not always effective in dealing with rapidly changing and dynamic conditions underwater. The optimization of inertia, propeller, battery capacity, and PID control characteristics proposed in this study shows that, although useful, PID control requires further adjustments to work efficiently under extreme environmental fluctuations. The numerical simulations performed also show that the AUV propeller often works in turbine mode, which requires additional protection for the AUV's electrical/electronic components, highlighting the need for more adaptive and robust control methods in underwater environments [15]

Previous research shows that advanced methods such as PID, EKF, and IMU control can improve depth control, but are often not fully effective under complex and dynamic environmental conditions [9-11]. Recent advances in the application of Lie Groups to robotic localization, such as the use of the Invariant Extended Kalman Filter (InEKF), have significantly improved the accuracy of estimation and characterization of uncertainty in underwater navigation. InEKF, which utilizes the dynamic error in the Lie Groups matrix, offers linearity with minimal approximation error and excellent convergence, enabling more effective integration of sensors such as IMU and DVL in navigation systems. Recent research integrating IMUs with sensor fusion systems and Invariant Extended Kalman Filter (InEKF)-based navigation techniques has shown improvements in stability and position estimation accuracy [16-17].

Although many solutions have been proposed for depth control, there is still an urgent need to develop a more adaptive and robust system in the face of uncertain environmental conditions, especially in underwater robotic applications such as SPIR. This research aims to integrate IMU with EKF to improve depth estimation accuracy and stability, and apply more adaptive PID control to deal with depth fluctuations more effectively. With this technology, it is expected that SPIR can achieve better stability, making a significant contribution to the safety and efficiency of underwater missions.

2. RESEARCH METHOD

To control the motor as the movement of SPIR, this research uses sensor stages such as Inertial Measurement Unit (IMU) and Extended Kalman Filter (EKF). The IMU is used to measure the linear acceleration and angular velocity of the robot, which provides information about the robot's position and orientation in space. The data obtained from the IMU is then processed using the EKF, which is a probability-based estimation technique to reduce noise and produce more accurate estimates of the robot's position and orientation. Controlling the estimation and movement of the robot is assisted by the PID method so that SPIR can move by adjusting the actuators used.

2.1. SPIR

SPIR (Submersible Pylon Inspection Robot) is an advanced technology specifically designed to facilitate movement and inspection below the water surface, especially in conditions that are difficult to reach by humans. The main focus of SPIR is its ability to maneuver in the underwater environment, using a series of thrusters and sensors. Movement on the SPIR (Submersible Pylon Inspection Robot) uses a configuration of four DC motors. Each motor has a specific role in controlling the horizontal and vertical motion of the robot, with the aim of improving stability and precision during underwater operations.

Motor 1 and Motor 2 (Horizontal Movement): The motors are placed at the back of the robot and configured to control forward and backward movements. The two motors work together to push the robot in a forward or backward direction, and differentially to perform turning maneuvers. Motor 3 and Motor 4 (Vertical Movement): The motors are mounted vertically and work to control the up and down

JURNAL ECTIPE
Electronic, Control, Telecommunication, Information, and Power Engineering
Volume 11, Issue 2, October 2024, pp. 224-234
ISSN 2355-5068 ; e-ISSN 2622-4852
DOI: 10.33019/jurnalecotipe.v11i2.4523

motion of the robot. By varying the rotation speed of these two motors, SPIR can adjust its depth in the water.

2.1. IMU

The positioning designer of the SPIR uses control principles on the x, y, and z axes. The x-axis determines the position or motion of the SPIR to the right and left, called surge motion, as well as rotation about the x-axis known as roll. On the y-axis, there is forward and backward movement called sway, and rotation about the y-axis called pitch motion. While in the z-axis, the SPIR position will form heave motion, which is the movement up and down in the z-axis direction, as well as rotation about the z-axis which determines the yaw position.

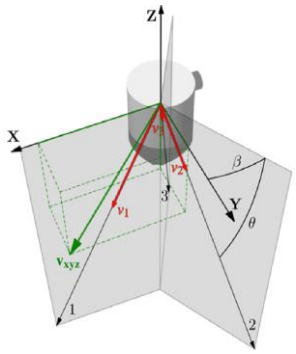

Figure 1. Axis of the IMU sensor

The propagation is described by a unit vector referenced to the sensor body frame and aligned with the transducer axis. The unit vector defines the relationship between these two velocities as:

$$v_i = e_i \cdot v_{xyz} \tag{1}$$

Where *vi* is a scalar value representing the speed measured by transducer I, **ei** is the unit vector corresponding to the same transducer and **vxyz** represents the vehicle speed in the sensor body frame:

$$v_{xyz} = [v_x \; v_y \; v_z \,] \tag{2}$$

In a three-transducer configuration, the unit vector is defined as

$$\begin{gathered} e_1 = [cos\ cos\ \theta \;\; -sin\theta \,] \\ e_2 = [-\cos\cos\theta \;\; sin\ sin\ \beta \;\; cos\ cos\ \theta\ cos\ cos\ \beta \;\; -sin\ sin\ \theta \;] \\ e_3 = [-\cos\cos\theta \;\; sin\ sin\ \beta \;\; \theta\ cos\ cos\ \beta \;\; -sin\ sin\ \theta \;] \end{gathered} \tag{3}$$

Then, the velocity measured on each beam can be obtained by substituting the unit vector:

$$\begin{aligned} v_1 &= v_x\ cos\ cos\ \theta \;-v_z\ sin\ sin\ \theta \;\; v_2 \\ &= -v_x\ cos\ cos\ \theta \;\; sin\ sin\ \beta \;+v_y\ cos\ cos\ \theta \;\; sin\ sin\ \beta \;-v_z\ sin\ sin\ \theta \;\; v_3 \\ &= \;-v_x\ cos\ cos\ \theta \;\; sin\ sin\ \beta \;-v_y\ cos\ cos\ \theta \;\; cos\ cos\ \beta \;-v_z\ sin\ sin\ \theta \end{aligned} \tag{4}$$

Finally, these three equations can be used to determine the three unknown components of vehicle speed.

$$\begin{aligned} v_x &= \frac{v_1}{cos\ cos\ \theta} + \frac{v_3 + v_2 + 2v_1\ sin\ sin\ \beta}{-2\ cos\ cos\ \theta \;-2\ cos\ cos\ \theta \;\; sin\ sin\ \beta} \quad v_y = \frac{v_2 - v_3}{2\ cos\ cos\ \theta\ cos\ cos\ \beta}\ v_z \\ &= \frac{v_3 + v_2 + 2v_1\ sin\ sin\ \beta}{-2\ sin\ sin\ \theta \;-2\ sin\ sin\ \theta\ sin\ sin\ \beta} \end{aligned} \tag{5}$$

The navigator aims to estimate the position of the robot. To achieve this goal, an interface known as the Navigation Sensor of the IMU is used. This interface provides various methods to return position, velocity, and acceleration in 6 DOF (Degree of Freedom) as well as an estimation of the quality of its measurements.

JURNAL ECTIPE
Electronic, Control, Telecommunication, Information, and Power Engineering
Volume 11, Issue 2, October 2024, pp. 224-234
ISSN 2355-5068; e-ISSN 2622-4852
DOI: 10.33019/jurnalecotipe.v11i2.4523

2.2. EKF

Extended Kalman Filter (EKF) is used to estimate the position, velocity, and orientation of SPIR by combining data from IMU and other sensors. EKF is a method capable of handling non-linear systems, which are often encountered in underwater navigation. The state equation describes the evolution of the system over time.

Extended Kalman Filter (EKF) is used to estimate the position, velocity, and orientation of an underwater vehicle (ROV) by combining data from IMU and other sensors. EKF is a method capable of handling non-linear systems, which are often encountered in underwater navigation. The state equations describe the evolution of the system over time:

$$x_{k+1} = f(x_k, u_k) + w_k \tag{6}$$

Where x_k is the state vector, u_k is the input vector and w_k is the process noise.

The observation equation describes how sensor measurements relate to the system state:

$$z_k = h(x_k) + v_k \tag{7}$$

Where z_k is the measurement vector and v_k is the measurement noise which is the algorithm of EKF with initialization.

$$\hat{x}_0 = x_0, P_0 = P_0 \tag{8}$$

Where $\hat{x}_0$ is the initial estimate of the state and P_0 is the initial error covariance matrix, with prediction.

$$\begin{aligned} \hat{x}_{k|k-1} &= f\left(\hat{x}_{k-1|k-1}, u_{k-1}\right) \\ P_{k|k-1} &= F_k P_{k-1|k-1} F_k^T + Q_k \end{aligned} \tag{9}$$

Where F_k is the Jacobian matrix of **f** with respect to x_k, and Q_k is the process noise covariance matrix. Update equations such as:

$$\begin{aligned} K_k &= P_{k|k-1} H_k^T \left(H_k P_{k|k-1} H_k^T + R_k\right)^{-1} \\ \hat{x}_k &= \hat{x}_{k|k-1} + K_k \left(z_k - h\left(\hat{x}_{k|k-1}\right)\right) \\ P_{k|k-1} &= (I - K_k H_k) P_{k|k-1} \end{aligned} \tag{10}$$

Where H_k is the Jacobian matrix of **h** exposed x_k and R_k is the measurement noise covariance matrix

2.3. Control System

Movement control is performed according to the desired direction. Once the data from the IMU and EKF is processed to estimate the position and orientation of the SPIR, the next step is to drive the motor or actuator to achieve the set goal. A PID (Proportional-Integral-Derivative) controller is used to generate the control signals required to drive the SPIR.

In this section, we define the basic parameters of SPIR (Submersible Pylon Inspection Robot) and the PID controller used in the simulation using MATLAB. The mass used is 10 Kg and with a damping coefficient that controls how fast the speed decreases due to friction or resistance of 0.5. The setpoint in this study is a depth of 5 meters. The simulation process is carried out in a loop with the following steps:

Calculating error

$$e(t) = depth - position\ (i-1) \tag{11}$$

Calculating integral and derivative errors

$$\begin{aligned} \text{Integral Error} &= \int_0^t e(\tau) d\tau \\ \text{Derivative Error} &= \frac{de(t)}{dt} \end{aligned} \tag{12}$$

Calculating the PID Control Signal

$$u(t) = K_p \cdot e(t) + K_i \cdot \int_0^t e(\tau) d\tau + K_d \cdot \frac{de(t)}{dt} \tag{13}$$

JURNAL ECOTIPE
Electronic, Control, Telecommunication, Information, and Power Engineering
Volume 11, Issue 2, October 2024, pp. 224-234
ISSN 2355-5068 ; e-ISSN 2622-4852
DOI: 10.33019/jurnalecotipe.v11i2.4523

SPIR Dynamics Model

$$a\,(i) = \frac{u\,(i) - c \cdot v(i-1)}{m} \tag{14}$$

$$v\,(i) = v(i-1) + a\,(i).\Delta t \tag{15}$$

$$x(i) = x\,(i-1) + v(i).dt \tag{16}$$

The output of the controller is an 8 bit PWM signal with $[0{,}255]$ or as $pwmrange$ with scale.

$$scaledoutputController = \frac{controlSignal - \min\,(controlSignal)}{\max(controlSignal) - \min(controlSignal)} \tag{17}$$

To make the duty cycle to signal the motor then.

$$Duty\ Cycle = \frac{scaledoutputController}{pwmrange} \tag{18}$$

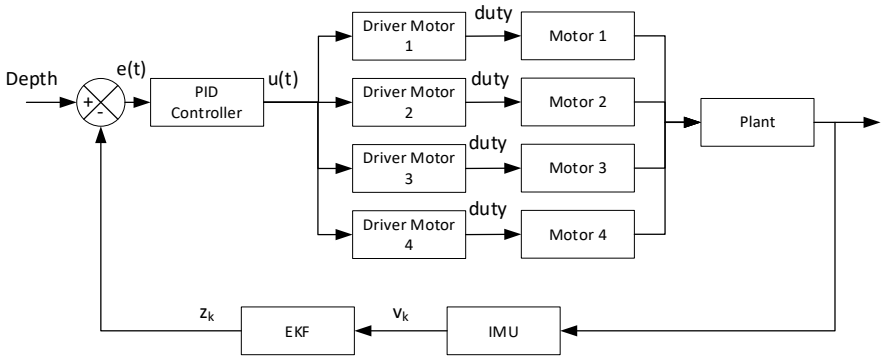

Figure 2. Overall block diagram

3. RESULTS AND DISCUSSION

In this chapter, we discuss the results of the analysis and implementation of controls for the Submersible Pylon Inspection Robot (SPIR) based on data obtained from various measurements and the mathematical equations used in the system. This discussion begins with an assessment of the system's accuracy in position estimation, continues with orientation and depth analysis, and concludes with an evaluation of the motor control.

3.1. Z Axis Position Error

Graph the position error on the Z-axis to evaluate the accuracy of the system in maintaining the desired depth. The equations used to calculate the velocity of the IMU, and the estimation results using the Extended Kalman Filter (EKF), will form the basis for understanding how this position error evolves over time.

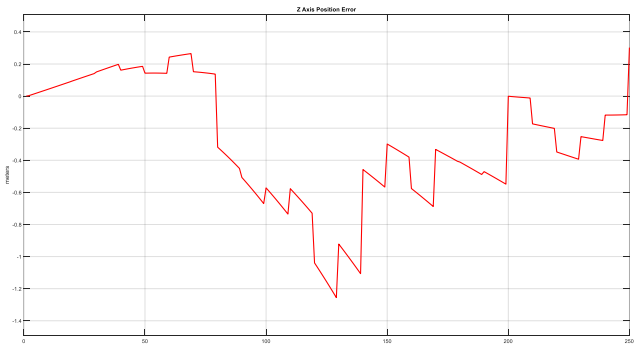

Figure 3. Error on the Z-axis

JURNAL ECTIPE
Electronic, Control, Telecommunication, Information, and Power Engineering
Volume 11, Issue 2, October 2024, pp. 224-234
ISSN 2355-5068; e-ISSN 2622-4852
DOI: 10.33019/jurnalecotipe.v11i2.4523

This figure illustrates the position error in the z-axis. At the beginning of the measurement, the position error starts from a value close to 0.5 meters and shows a significant decrease with some large fluctuations. The position error reaches its lowest value of about -1.5 meters at the 100th step, indicating a large error in position estimation at that phase. After reaching the lowest point, the position error starts to increase again, albeit with smaller fluctuations. The figure above shows that the system experiences large fluctuations in the early stages of measurement, both in quaternion angle and in position estimation. The correlation between quaternion angle fluctuations and position error may indicate that the stability of the quaternion angle contributes to the reduction of position error over time.

3.2. Quaternion distance

Furthermore, the quaternion angle graph is displayed to check the stability of the SPIR orientation. The quaternion angle provides information about the rotation and orientation of the SPIR during the simulation, which is a key factor in ensuring that the position and depth estimates are accurate. This data is important for understanding the effect of orientation on position error and how orientation stability contributes to depth control.

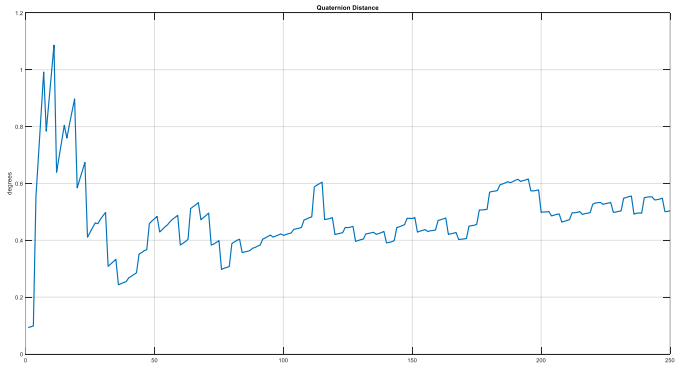

Figure 4. Quaternion distance

In the analysis of the resulting data, it shows significant variations at the start of the measurement. The large fluctuations seen in this plot, with peaks reaching about 1.1 degrees, are due to the initial instability of the sensor. After the initial fluctuation period, the quaternion angle shows a tendency to stabilize with small fluctuations that persist until the end of the measurement.

3.3. Depth Position

The depth position graph shows the change in SPIR depth over time. This graph provides immediate context on how the system responds to depth control and relates it to previously identified position errors. The depth position analysis allows us to assess the effectiveness of the control in practice and see how the desired depth is achieved or maintained.

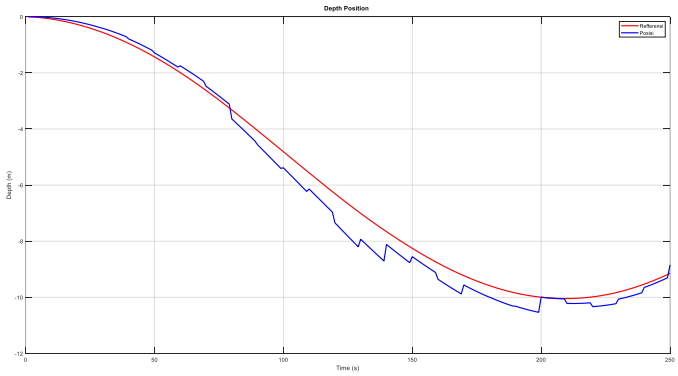

Figure 5. Depth position

JURNAL ECTIPE
Electronic, Control, Telecommunication, Information, and Power Engineering
Volume 11, Issue 2, October 2024, pp. 224-234
ISSN 2355-5068 ; e-ISSN 2622-4852
DOI: 10.33019/jurnalecotipe.v11i2.4523

In the initial phase of measurement (0 to 50 seconds), the actual depth generally follows the reference depth accurately, although there is a slight deviation. However, after 50 seconds, the deviation between the actual and reference depths began to increase, with the actual depth showing greater fluctuations than the reference. At a depth of about -6 meters, the deviation becomes more significant, and at a maximum depth of about -10 meters, there is the greatest deviation, with the actual depth far below the reference line. This shows the difficulty of the system in maintaining the desired depth at deeper depths.

After reaching the deepest depth, both the actual and reference depths started to return to shallower depths, with the actual depth still showing fluctuations but getting closer to the reference depth. Overall, while SLAM can follow the reference depth at shallower depths quite well, the system shows limitations in maintaining a stable depth at deeper depths.

In addition, the performance of the system combining the Inertial Measurement Unit (IMU) and Extended Kalman Filter (EKF) is shown to improve the accuracy of depth and position estimation. In the Z-axis position error graph, it can be seen that the large fluctuations in the initial phase of measurement are minimized over time thanks to better system calibration. The IMU is able to provide fairly accurate data on acceleration and angular velocity, while the EKF is effective in filtering out noise and integrating data from multiple sensors to provide more stable position estimation. Even so, challenges remain at deeper depths, where the deviation from the reference depth becomes larger. This signals the need for further customization of the system to deal with more extreme environmental conditions.

3.4 SPIR Robot Movement Depth

This motor is for depth regulation, and this graph shows how the PID control signal is translated into motor motion. This evaluation helps in assessing how well the depth control is controlled by the motor.

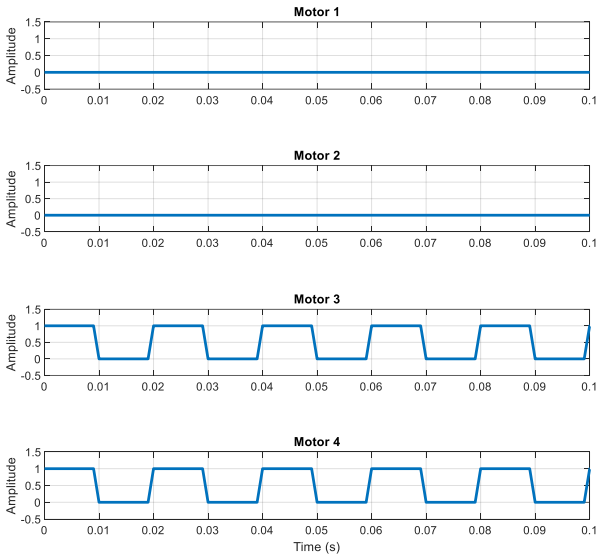

Figure 6. Depth movement of the SPIR robot

The figure above shows the activity of the four motors depicted through the change in amplitude against time. In the first and second subplots, it can be seen that motor 1 and motor 2 show no significant change in amplitude, remaining around zero all the time. This indicates that motor 1 and motor 2 are inactive or stopped, with no PWM (Pulse Width Modulation) applied to them.

In contrast, in the third and fourth subplots, there is a clear and oscillating change in amplitude, indicating that motor 3 and motor 4 are active. This changing amplitude indicates that the presence of PWM indicates that motors 3 and 4 are rotating. The activity of motors 3 and 4 indicates that they are operating to reach a certain depth according to the given PWM pattern, while motors 1 and 2 remain inactive.

JURNAL ECTIPE
Electronic, Control, Telecommunication, Information, and Power Engineering
Volume 11, Issue 2, October 2024, pp. 224-234
ISSN 2355-5068; e-ISSN 2622-4852
DOI: 10.33019/jurnalecotipe.v11i2.4523

The motor activity in SPIR shows specific coordination for the stabilization and depth regulation tasks. Motor 1 and Motor 2 remain inactive during depth setting operations, as these motors function to maintain horizontal stability (roll and pitch). Meanwhile, Motor 3 and Motor 4 are active in controlling the vertical movement, which allows SPIR to achieve and maintain the desired depth. This pattern shows the logic behind the motor assignment, where the depth drive motors are focused on setting the vertical position, while the stabilization motors function in maintaining balance when there is no significant depth change.

3.5. SPIR Robot Motion to Maintain Special Stability of Motors 1 and 2

Analyze the motion graphs of motors 1 and 2 that stabilize the SPIR. This graph illustrates how these motors operate to stabilize the SPIR and maintain balance, as well as ensuring that the system can cope effectively with changes in position and depth. This evaluation provides a complete view of how position stabilization is maintained and how the overall control is implemented.

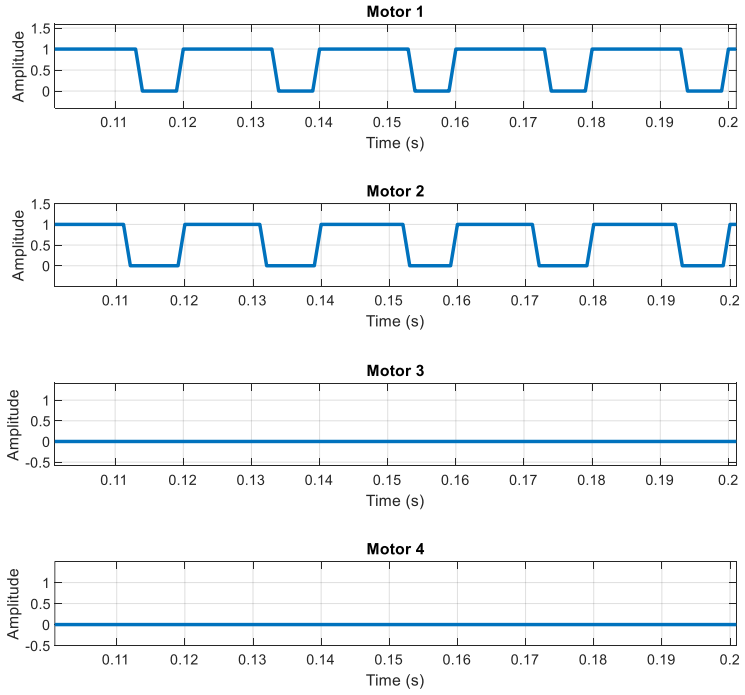

Figure 7: Movement to maintain depth position

This figure shows the activity of four motors in an attempt to maintain a certain depth, focusing on motor 1 and motor 2. In the first and second subplots, it can be seen that motor 1 and motor 2 experience significant amplitude changes and oscillate between certain values. This pattern indicates that motor 1 and motor 2 are active and rotating, following the given PWM (*Pulse Width Modulation*) signal. This activity of motors 1 and 2 indicates that they are functioning to maintain the desired depth by regulating their rotation speed and direction based on the PWM pattern.

In contrast, the third and fourth subplots show that motor 3 and motor 4 were not active during this observation period, as the amplitude remained around zero all the time. The absence of amplitude change in motor 3 and motor 4 indicates that no PWM signal was applied.

4. CONCLUSION

This research has shown that the integration of Inertial Measurement Unit (IMU) and Extended Kalman Filter (EKF) as well as the use of customized PID control provide improvements in the depth control of the Submersible Pylon Inspection Robot (SPIR). However, test results show that large fluctuations at deeper depths, especially around 6 to 10 meters, require more specific refinement of the control algorithm. To improve stability and accuracy at more extreme conditions, refinements to the PID control algorithm are required. These enhancements could be the application of advanced control or

Volume 11, Issue 2, October 2024, pp. 224-234
ISSN 2355-5068 ; e-ISSN 2622-4852
DOI: 10.33019/jurnalecotipe.v11i2.4523

even predictive model-based control to adapt the system response to rapid changes in underwater current and depth fluctuations. In addition, the performance of the IMU and EKF in this system shows good results under normal conditions, but significant challenges arise when the system encounters sensor noise, especially in the early phase of measurement. Large fluctuations in the quaternion angle due to the initial instability of the sensor contribute to the initial estimation error. To address this issue, it is recommended to make adjustments to the EKF parameters and consider the use of additional filters that can accelerate convergence and reduce noise in the sensor data. Overall, this research has contributed to developing more accurate depth control in SPIR. However, the next step involves improving the PID control algorithm as well as refining the integration of IMU and EKF, especially to deal with dynamic and fluctuating underwater environmental conditions at greater depths.

ACKNOWLEDGMENTS

This research is supported by funding from the Academic Directorate of Vocational Education and the Research and Service Center (P3M) of Cilacap State Polytechnic. We would like to thank all parties who have provided support and contributions in the implementation of this research. The support we receive is very meaningful in realizing the development of the technology we study.

REFERENCES

[1] E. Zereik, M. Bibuli, N. Mišković, P. Ridao, and A. Pascoal, "Challenges and future trends in marine robotics," *Annu Rev Control*, vol. 46, no. October, pp. 350–368, 2018, doi: 10.1016/j.arcontrol.2018.10.002.

[2] Scmidt iotc 2021, *Membaca Pesan Komandan KRI Nanggala-402*. 2021, p. 6.

[3] J. Collins, S. Chand, A. Vanderkop, and D. Howard, "A Review of Physics Simulators for Robotic Applications," *IEEE Access*, vol. 9, pp. 51416–51431, 2021, doi: 10.1109/ACCESS.2021.3068769.

[4] C. Li *et al.*, "An Underwater Image Enhancement Benchmark Dataset and Beyond," *IEEE Transactions on Image Processing*, vol. 29, pp. 4376–4389, 2020, doi: 10.1109/TIP.2019.2955241.

[5] M. J. Islam, Y. Xia, and J. Sattar, "Fast Underwater Image Enhancement for Improved Visual Perception," *IEEE Robot Autom Lett*, vol. 5, no. 2, pp. 3227–3234, 2020, doi: 10.1109/LRA.2020.2974710.

[6] K. Le, A. To, B. Leighton, M. Hassan, and D. Liu, "" The SPIR: An Autonomous Underwater Robot for Bridge Pile Cleaning and Condition Assessment," 2021. [Online]. Available: https://www.youtube.com/watch?v=uz1ZXV5Oths.

[7] N. Nomikos, P. K. Gkonis, P. S. Bithas, and P. Trakadas, "A Survey on UAV-Aided Maritime Communications: Deployment Considerations, Applications, and Future Challenges," *IEEE Open Journal of the Communications Society*, vol. 4, pp. 56–78, 2023, doi: 10.1109/OJCOMS.2022.3225590.

[8] P. Trslic *et al.*, "Vision based autonomous docking for work class ROVs," *Ocean Engineering*, vol. 196, p. 106840, 2020, doi: https://doi.org/10.1016/j.oceaneng.2019.106840.

[9] Y. Batmani and S. Najafi, "Event-Triggered H∞ Depth Control of Remotely Operated Underwater Vehicles," *IEEE Trans Syst Man Cybern Syst*, vol. 51, no. 2, pp. 1224–1232, 2021, doi: 10.1109/TSMC.2019.2896382.

[10] R. Gabl *et al.*, "Hydrodynamic loads on a restrained ROV under waves and current," *Ocean Engineering*, vol. 234, p. 109279, 2021, doi: https://doi.org/10.1016/j.oceaneng.2021.109279.

JURNAL ECTIPE
Electronic, Control, Telecommunication, Information, and Power Engineering
Volume 11, Issue 2, October 2024, pp. 224-234
ISSN 2355-5068; e-ISSN 2622-4852
DOI: 10.33019/jurnalecotipe.v11i2.4523

[11] M. Dong, J. Li, and W. Chou, "Depth control of ROV in nuclear power plant based on fuzzy PID and dynamics compensation," *Microsystem Technologies*, vol. 26, no. 3, pp. 811–821, 2020, doi: 10.1007/s00542-019-04605-x.

[12] A. Bucci, L. Zacchini, and A. Ridolfi, "EKF on Lie Groups for Autonomous Underwater Vehicles orientation initialization in presence of magnetic disturbances," in *2022 IEEE/OES Autonomous Underwater Vehicles Symposium (AUV)*, 2022, pp. 1–6. doi: 10.1109/AUV53081.2022.9965905.

[13] H. Xing *et al.*, "A Multi-Sensor Fusion Self-Localization System of a Miniature Underwater Robot in Structured and GPS-Denied Environments," *IEEE Sens J*, vol. 21, no. 23, pp. 27136–27146, 2021, doi: 10.1109/JSEN.2021.3120663.

[14] H. Li, S. Chang, Q. Yao, C. Wan, G.-J. Zou, and D.-L. Zhang, "Robust Heading and Attitude Estimation of MEMS IMU in Magnetic Anomaly Field Using a Partially Adaptive Decoupled Extended Kalman Filter and LSTM Algorithm," *IEEE Trans Instrum Meas*, vol. 73, pp. 1–13, 2024, doi: 10.1109/TIM.2024.3381659.

[15] P. V. Patil, M. K. Khan, M. Korulla, V. Nagarajan, and O. P. Sha, "Design optimization of an AUV for performing depth control maneuver," *Ocean Engineering*, vol. 266, p. 112929, 2022, doi: https://doi.org/10.1016/j.oceaneng.2022.112929.

[16] E. R. Potokar, K. Norman, and J. G. Mangelson, "Invariant Extended Kalman Filtering for Underwater Navigation," *IEEE Robot Autom Lett*, vol. 6, no. 3, pp. 5792–5799, 2021, doi: 10.1109/LRA.2021.3085167.

[17] P. Trslic *et al.*, "Vision based autonomous docking for work class ROVs," *Ocean Engineering*, vol. 196, p. 106840, 2020, doi: https://doi.org/10.1016/j.oceaneng.2019.106840.